Modulated-laser source induction system for remote detection of infrared emissions of high explosives using Laser-Induced Thermal Emission (LITE)

Nataly J. Galán-Freyle[a,b], Leonardo C. Pacheco-Londoño[a,b*] Amanda M. Figueroa-Navedo[c], William Ortiz-Rivera[a,d], John R. Castro-Suarez,[a,e] and Samuel P. Hernández-Rivera[a*]

[a]ALERT DHS Center of Excellence for Explosives Research, Department of Chemistry, University of Puerto Rico-Mayaguez Campus, Mayagüez, PR 00681, USA

[b]School of Basic and Biomedical Science, Universidad Simón Bolívar, Barranquilla 080002, Colombia

[c]Department of Chemistry and Chemical Biology, Northeastern University, 360 Huntington Avenue, Boston, MA 02115, USA

[d]University of Puerto Rico- Bayamón Campus, Bayamón, PR 00959, USA

[e]Exact Basics Area, Universidad del Sinú, Unisinú, Cartagena, Colombia.

Abstract

In a homeland security setting, the ability to detect explosives at a distance is a top security priority. Consequently, the development of remote, non-contact detection systems continues to represent a path forward. In this vein, a remote detection system for excitation of infrared emissions using a CO_2 laser for generating Laser-Induced Thermal Emission (LITE) is a possible

23 solution. However, a LITE system using a CO_2 laser has certain limitations, such as the

24 requirement of careful alignment, interference by the CO_2 signal during detection, and the power

25 density loss due to the increase of the laser image at the sample plane with the detection distance.

26 In this study, a remote chopped-laser induction system for LITE detection using a CO_2 laser

27 source coupled to a focusing telescope was built to solve some of these limitations. Samples of

28 fixed surface concentration (500 $\mu g/cm^2$) of 1,3,5-trinitroperhydro-1,3,5-triazine (RDX) were

29 used for the remote detection experiments at the distance ranging between 4 and 8 m. This

30 system was capable of thermally exciting and capturing the thermal emissions (TEs) at different

31 times in a cyclic manner by a Fourier Transform Infrared (FTIR) spectrometer coupled to a gold-

32 coated reflection optics telescope (FTIR-GT). This was done using a wheel blocking the capture

33 of TE by the FTIR-GT chopper while heating the sample with the CO_2 laser. As the wheel

34 moved, it blocked the CO_2 laser and allowed the spectroscopic system to capture the TEs of

35 RDX. Different periods (or frequencies) of wheel spin and FTIR-GT integration times were

36 evaluated to find dependence with observation distance of the maximum intensity detection,

37 minimum S/N ratio, CO_2 laser spot size increase, and the induced temperature increment (ΔT).

38

Keywords

42

43 ***Leonardo C. Pacheco-Londoño & Samuel P. Hernández-Rivera:** E-mail:

44 leonardo.pacheco@upr.edu; samuel.hernandez3@upr.edu

1 Introduction

Laser-Induced Thermal Emission (LITE)[1-7] detection of analytes is an important remote detection technique for monitoring hazardous chemicals safely.[8-25] In a homeland security setting, the detection of high explosives (HEs) enabled by LITE spectroscopy could play an important role in maintaining safe operations while conducting real-time detection and fast analysis.[26-30] However, the limits of the detection (LOD) depend on the source to target distance, on the laser power, on the divergence of the source, as well as on the collection efficiency and detector sensitivity.[31] Several studies have demonstrated that the use of a CO_2 laser as an excitation source for LITE spectroscopy at long distances is highly suitable for stimulating strong IR emissions of analytes of interest, such as trace amounts of HEs.[1,12,32-34] This feasibility of detection and identification of small quantities of HEs on surfaces is enabled by the fact that CO_2 lasers operate in the mid-infrared (MIR), i.e., in the fingerprint region. HEs have strong vibrational signatures in the MIR that can lead to generate resonant absorption by the analytes. MIR radiation is strongly absorbed by the analyte, leading to relatively high local temperatures. Thus, LITE spectroscopy is a technique that has many advantages: the sample itself is the source of the analytical information,[32,35] a strong resonant infrared photothermal approach,[31] and the facility for detecting other threat chemicals regardless of size, shape, and substrate type.

In a previous study developed by our research group, low surface concentrations of samples of HEs were thermally excited to higher vibrational energy levels using a CO_2 laser, and the radiant relaxation process was monitored using a telescope-coupled FTIR interferometer.[1,36] The emission spectra of HE: TNT, DNT, PETN, TATP, and RDX were successfully monitored at distances from 4 to 64 m. During these experiments, several problems were identified. First, the telescope should have been configured with a shutter to avoid blinding the detector due to the

68   back reflection of the laser beam. Second, the spectra were collected during the time interval in

69   which the sample was cooling after the laser was turned off. Third, the laser irradiance decreased

70   with the source-target distance because the laser spot (LS) size increased. The induced local

71   temperatures (ΔT) at each laser-target range (4, 8, 16, 32, and 64 m) were 72, 20, ~7, ~3, and > 1

72   ºC. It was proposed that better results could be obtained by collimating the laser to increase the

73   ΔT and obtain higher emission levels. Fourth, careful alignment of the laser-target-detector angle

74   was necessary when the telescope and the excitation source are not part of the same device.

75   Therefore, the main objective of this study was to develop a new experimental set-up for remote

76   LITE detection of HEs and proposing a methodology that allows solving these four problems

77   that affect the experimental efficiency of LITE spectroscopy.

78

79   ## 2   Methodology

80   *2.1 Sample preparation*

81   Only one HE was used in the experiments: 1,3,5-trinitroperhydro-1,3,5-triazine (RDX) which

82   was synthesized in the laboratory. Acetone (99.5%, GC grade, Thermo-Fisher Scientific,

83   Waltham, MA, USA) was used as the solvent. RDX samples were deposited on aluminum plates

84   substrates (Al: 2.54 cm $\times$ 2.54 cm) at a nominal surface concentration of 500 $\mu g/cm^2$. A sample-

85   smearing technique was used to deposit the RDX samples.[37,38] A stock solution of RDX was

86   prepared in acetone. A Teflon® stub (3 cm wide and 0.04 cm thick) was used to smear a fixed

87   volume (10 μL) of the solutions containing the analytes onto the metal surface. The smearing

88   was performed quickly, tilting the Teflon® sheet to the right or left in a single-pass operation. A

89   minimal adhesion of 500 $\mu g/cm^2$ to the Teflon was assumed. The plates were first cleaned with

90   acetone followed by air-drying before the desired RDX surface loading was deposited.

91   *2.2 Apparatus*

92   The experimental setup used is illustrated in Fig. 1. It consisted of an intermittent excitation

93   system of the thermal emissions (TE) induced by a CO_2 laser as the excitation source. This

94   system was capable of thermally exciting and acquiring the TE at different times in a cyclic

95   manner using a Fourier transform infrared (FTIR) spectrometer coupled to a gold-coated optics

96   reflective telescope (GT). The chopping of the laser beam was accomplished using a wheel to

97   block the laser and the capture of the TE by the FTIR-GT while heating the sample with the CO_2

98   laser. As the wheel moved, it blocked the CO_2 laser and allowed the acquisition of the TEs by the

99   FTIR-GT. The sample temperature was measured with a thermocouple thermometer. On   the

100   back of the aluminum plate that was used as sample substrate, a cylindrical cavity was drilled

101   close to the surface of the samples and the thermocouple head was fixed in place. This reduced

102   the temperature difference between the sample and thermocouple by less than 0.5 ºC.

103   *2.2.1 Telescope*

104   The catadioptric telescope used was an Argunov-Cassegrain design, equipped with gold-coated

105   mirrors. The primary and secondary mirrors were 15 cm and 5 cm in diameter, respectively. The

106   telescope was modified by allowing the secondary mirror to move and form an image at the focal

107   plane from infinite distance to less than 4 m. This was possible by placing the secondary mirror

108   in a movable optical mount (movement represented by a dotted arrow in Fig. 1) with a linear

109   displacement resolution of 1 μm to allow the decreased focal point of the reflective system.[1]

110   *2.2.2 Spectrometer*

111   The infrared spectrometer used was an open-path-FT-IR interferometer, model EM27 (Bruker

112   Optics, Billerica, MA, USA). The optical bench consisted of a compact, enclosed, and desiccated

113   Michelson-type interferometer equipped with ZnSe windows, an internal blackbody (BB)

114   calibration source, a KBr beamsplitter, a very fast native focal ratio of f/0.9 with a field of view

115   (FOV) of 30 mrad (1.7°). The FOV was reduced to 10 mrad (0.6°) by the receiver telescope,

116   which had an infinite focal point magnification of 3×.[1]

117   *2.2.3 Optical chopper wheel (OCW)system*

118   The optical chopper wheel (OCW) used consisted of an aluminum plate cut to a radius of 15.2

119   cm which had a two-and-a-half arc-shaped opening (slightly larger than the spectrometer

120   window) and an angle of 153.5° (Fig. 1(a)). The wheel contained a counterweight on the side of

121   the opening with its center of mass at the center of the wheel so that when turning, it would not

122   pivot.

123   *CO_2 laser*: The target surface was heated using a CO_2 laser with 36 W as maximum output

124   power (Firestar vi30, Synrad, Inc., Mukilteo, WA, USA), and an emission band from 926 to 980

125   cm^{-1}. The laser beam was aligned with the center of the spectrometer window in an imaginary

126   line called "the horizon." The center of the telescope mirror was aligned with the center ray of

127   the laser beam. The laser radiation was reflected by two plane gold-coated mirrors to enter the

128   telescope. Then, the laser beam was reflected towards the secondary mirror of the telescope and

129   then to the primary mirror and then onto the sample (Fig. 1). This strategy of using the telescope

130   to focus the laser light ensures that the LS on the sample was small and the laser power was high

131   to ensure a strong heating effect. Thus, the telescope assumed two roles, focusing the laser and

132   collecting the emission. Moreover, the alignment with respect to the sample was minimal and

133   was only necessary to point at the sample plane. A 532 nm laser pointer was used to align the

134 path of the CO_2 laser to aim the sample. This part of the system contained a moving mirror that

135 allowed pointing to the sample. This mirror is removed to start the LITE detection.

136 *2.2.4 Time-step*

137 The OCW system divided the cycle into four-time steps (Fig. 1(b)). The first step was the

138 acquisition time. In this time, the OCW rotated 153.5º allowing the telescope to capture the

139 emissions and then passing through to the spectrometer and, at the same time, blocking the CO_2

140 laser. The second step was a transition time. In this period, the OCW opened to a 26.5º arc and

141 completely blocked the CO_2 laser letting the spectrometer window partially. In the third time

142 step, the OCW rotated by 153.5º, letting the laser light pass towards the telescope and blocking

143 the window of the spectrometer so that it did not detect the laser light when it was heating the

144 sample. Finally, in the fourth step consisted of a secondary transition time in which the OCW

145 turned by 26.5º, remaining to block the CO_2 laser while the spectrometer window was partially

146 closed.

147

148 **3 Results**

149 *3.1 Relative IR thermal emission of the OCW*

150 In the first set of experiments, samples of RDX of 500 $\mu g/cm^2$ nominal surface loading were

151 placed at a target distance 4 m from the cyclic induction system. The target samples were

152 focused by the telescope using the laser pointer. Next, the OCW was adjusted to a wheel

153 frequency (f_w) of 0.1 Hz, and the spectra were acquired with an integration time (t_i) of 2.0 s,

154 continuously. Fig. 2 (a) shows the profiles of the emission spectra. Two types of spectra were

155 acquired, emission spectra of the samples with the OCW switched off (Off), and sample

156 emission spectra of the samples with the OCW switched on (On). These are illustrated in Fig. 2

157 (a) by red and black traces, respectively. The ratios between these two types spectra were

158 calculated and called relative emission spectra (On/Off ratios or e_A) with respect to the aluminum

159 OCW at room temperature used as background.

160   In Fig. 2(a), the e_A spectrum of RDX (purple trace) reveals the characteristic spectral pattern

161 for RDX as can be observed in relation to an emissivity spectrum of RDX used reference to a

162 standard of RDX (green trace). Usually, the relative emission spectrum is obtained by dividing

163 the emission of the sample by the emission of the blackbody at the same temperature as the

164 sample. This situation generates an inverted signal spectrum since the blackbody emission is

165 always higher than the sample emission, but in this case, e_A spectra were obtained with respect to

166 the emission of the aluminum OWC. However, the chopper wheel material does not behave as a

167 blackbody, and its emission temperature is lower than the sample emission temperature. This has

168 the effect that the vibrational features in the spectrum are shown upward looking (as if it were an

169 absorption spectrum). This practical form of detection is convenient since, in the case of remote

170 detection in the field, the temperature of the sample is unknown. For that reason, this work has

171 been focused on making the detection considering the possibility of applications in real

172 scenarios.

173   The MIR signals for RDX that stand out include the band at 1234 cm^{-1} and the band at 1034

174 cm^{-1} for N-C-N stretch, the signals at 1016 $cm^{-1,}$ and 943 cm^{-1} for the combination N-NO$_2$ stretch

175 and in-plane C–H bending, respectively. Other RDX signatures identified are 919 cm^{-1} out-of-

176 plane CH$_2$ bending, the ring breathing mode at 881 cm^{-1}, the band at 850 cm^{-1} for C-N-C stretch,

177 and the band at 779 cm^{-1} for N-C-N stretch.[39,40] The band at 1321 cm^{-1} for N-NO$_2$ symmetric

178   stretch and the signal at 1593 cm^{-1} for the N-NO$_2$ asymmetric stretch were not observed because

179   water vapor signals overshadowed them (Fig 1(a)).

180   Fig. 2(b) shows the e$_A$ spectra for 18 cycles of the OCW at fw = 0.1 Hz. The inserted figure

181   shows the time step for this experiment, where the t$_i$ was 2.0 s. The asterisks indicate the

182   spectrum used to obtain e$_A$. The increase of the characteristic emission RDX signals was

183   observed due to the increase in sample temperature.

184   *3.2 Signal monitoring of the OCW adjusted by frequency and integration time*

185   Samples of 500 µg/cm^2 of RDX were placed at 4 m of distance from the cyclic thermal induction

186   system and focused onto the FOV of the telescope using the laser pointer. A background

187   spectrum of aluminum of OCW was initially acquired. Next, the f$_w$ of the OCW system was

188   adjusted to 0.1, 0.2, 0.4, 1.0, and 2.0 Hz and acquiring spectra with a t$_i$ of 2.0 s, continuously.

189   Then, the f$_w$ was set at 1.0 Hz, and the t$_i$ was varied between 0.5 to 2.2 s. In Fig. 3(a-d) the e$_A$ for

190   the RDX signal at 1234 cm^{-1} at 100 s are shown, with a total of 50 spectra for different f$_w$ values.

191   Three types of points are shown: blue diamond represent spectra in Off mode (when the wheel

192   obstructs the spectrometer window); red diamond represent spectra in On mode (when the

193   spectrometer window is clear), and green diamond are intermediate between On and Off

194   positions. In Fig. 3(d) when the spectra acquisition of the OCW was adjusted to t$_i$ = 2.0 s and f$_w$

195   2.0 Hz, the cyclic speed increase was evidenced. Therefore, the OCW would enable the

196   acquisition of four spectra in the On position and four spectra in the Off position. Consequently,

197   each green diamond represents the average of the e$_A$ at 1234 cm^{-1} for RDX of all spectral

198   acquisitions in On and Off (On-Off) time. Fig 3 (a) shows only the e$_A$ for the peak at 1234 cm^{-1}

199   in On and Off due to cyclic speed decrease.

200   Fig. 4(a) shows the e_A spectra #50 for different f_w in contrast with the standard spectra of

201   RDX (solid black line). In all e_A spectra, the characteristic signals of RDX were observed.

202   However, the best spectra e_A were observed at f_w values of 0.2 and 0.4 Hz due to the decrease of

203   the noise in the spectra. Although RDX signals in the e_A spectra for 0.1 Hz are very intense, they

204   also contain a higher noise compared to other spectra.

205   The effect of the integration time (t_i)was also evaluated. In this case, the cyclic system was

206   set at f_w 1.0 Hz and t_i was varied between 0.5 to 2.2 s. Fig. 4(b) shows the spectra with higher

207   intensity (max) and less intensity (min) and their spectral average (Av), varying the t_i: 0.54 s,

208   1.08 s, and 2.16 s. In general, for all Av spectra, the t_i values evaluated showed a variation in the

209   spectral pattern that represents the RDX spectrum was observed. However, the increase in t_i

210   allows that the OCW acquires enough sample information to get a good signal for both max and

211   min spectra.

212   *3.3 Dependence of CO_2 laser spot and ΔT with the distance*

213   The dependence of the LS diameter of the CO_2 laser and the induced temperature increment (ΔT)

214   by the LITE process on RDX samples was investigated. The LS diameter of the CO_2 laser was

215   determined to increase by 0.5 cm/meter without a focusing telescope (Galán-Freyle et al.[1]). In

216   contrast, when the telescope was used to focus the LS the increase in diameter was only 0.1

217   cm/meter. LS diameter as a function of distance was measured using thermal paper (change in

218   color with temperature). For the measurements, thermal paper was exposed to the laser action for

219   5 s, leaving a stain of the size of the LS diameter. The measurements were repeated for 5 times

220   and an average was calculated. The uncertainty of the reported diameter values was $\pm$ 0.05 cm.

221   This reduced increment in LS diameter was reflected in the ΔT induced and the signal

222   dependence with source-target distance. The results are shown as insets of Fig. 5(a). Focusing

223   the LS with the telescope for LITE detection at 4 m induced a ΔT lower than LITE detection

224   without a telescope. This result is attributed to the fact that in the present optical arrangement,

225   the induced heat transfer is an intermittent process.

226   When the sensing distance increased to 8 m, the effect of the increase of the LS diameter per

227   meter is more evident. The ΔT for LITE detection without focusing the LS decreases

228   approximately 50 ºC in comparison with focusing the LS in which the decrease in ΔT is

229   maintained almost to 10 ºC, as shown on the right side inset of Fig. 5 (a). A fit was obtained

230   between the ΔT induced at the sample and the reciprocal of the LS diameter (shown on left side

231   inset of Fig. 5 (a)). The dependence obtained is as expected because when increasing the LS

232   diameter, the power per unit area decreases, generating a lower ΔT.

233   To evaluate the effect of the telescope as a focusing tool in remote detection using a LITE

234   intermittent induction system, a comparison was made with the report by Galán-Freyle et al.,[1]

235   using the RDX samples deposited on Al substrates at the same nominal surface concentration

236   (500 $\mu g/cm^2$). The signal to noise ratio (S/N) for the RDX samples was measured and compared

237   between LITE systems with and without focusing the LS with the telescope. Fig. 5(b) shows the

238   averages of e_A for RDX spectra acquired with the cyclic induction LITE system at 4, 6, and 8 m

239   of source-target distances. The inset in Fig. 5(b) shows that at 4 m of source-target distance, a

240   higher S/N ratio was achieved by the non-focused LITE system. However, at 8 m of source-

241   target distance, the S/N ratio was higher for the cyclic induction LITE system focusing the LS

242   with the telescope system.

243

4   Conclusion

244

245   The proposed methodology showed an improved efficiency in the alignment of the LITE process

246   at the sample plane. The dependence of LITE with source-target distance was improved, solving

247   the excessive increase in the size spot of the CO_2 laser in the LITE process. The sample emission

248   rate was measured without the interference of the CO_2 laser light. The optimum conditions for

249   the cyclic induction LITE system were adjusted to 1 Hz for the frequency of the chopper wheel

250   and an integration time of 2.0 s. In this study, only LITE detection distances from 4 to 8 m were

251   evaluated. For future work, it is expected to investigate at a longer detection distances, with other

252   sources of excitation such as tunable MIR lasers (quantum cascade lasers), synchronizing the

253   detector with the chopper.

254   It is emphasized that it was not necessary to measure the temperature of a blackbody or to

255   have to turn off the laser because it saturated the detector. This is a definite advantage of cyclic

256   induction LITE systems making it more amenable real field applications.

257

265　and should not be interpreted as necessarily representing the official policies, either expressed or

266　implied, of the U.S. Department of Homeland Security.

267

268　**References**

269　1.　N. J. Galán-Freyle et al., "Standoff Detection of Highly Energetic Materials Using Laser-

270　　　Induced Thermal Excitation of Infrared Emission," *Applied Spectroscopy* **69**(5), 535-544

271　　　(2015).

272　2.　L. T. Lin, D. D. Archibald, and D. E. Honigs, "Preliminary Studies of Laser-Induced

273　　　Thermal Emission Spectroscopy of Condensed Phases," *Appl. Spectrosc.* **42**(3), 477-483

274　　　(1988).

275　3.　W. M. Michael J. Wilhelm, Jonathan M. Smith, Hai Lung Dai, "The lowest quartet-state of

276　　　the ketenyl (HCCO) radical: Collision-induced intersystem crossing and the v2 vibrational

277　　　mode," *Chemical Physics.* **422**(290-296 (2013).

278　4.　M. N. Michael J. Wilhelm, Laura Letendre, Hai Lung Dai, "Photodissociation of vinyl

279　　　cyanide at 193 nm: Nascent product distributions of the molecular elimination channels," *J.

280　　　Chem. Phys* **130**(4), (2009).

281　5.　L. T. Letendre et al., "Time-Resolved FTIR Emission Spectroscopy of Transient Radicals," *J.

282　　　Chinese Chem* **52**(4), 677-686 (2005).

283　6.　L. T. Letendre et al., "Interfacing a transient digitizer to a step-scan Fourier transform

284　　　spectrometer for nanosecond time resolved spectroscopy," *Rev. Sci. Instrum* **70**(1), 18-22

285　　　(1999).

286　7.　V. Karpovych et al., "Laser-induced thermal emission of rough carbon surfaces," *Journal of

287　　　Laser Applications* **32**(1), 012010 (2020).

288   8. S. Wallin et al., "Laser-based standoff detection of explosives: a critical review," *Anal.*
289   *Bioanal. Chem* **395**(2), 259-274 (2009).

290   9. C. W. Van Neste, L. R. Senesac, and T. Thundat, "Standoff Spectroscopy of Surface
291   Adsorbed Chemicals," *Anal. Chem* **81**(5), 1952-1956 (2009).

292   10. L. Pacheco-Londoño et al., "Vibrational spectroscopy standoff detection of explosives," *Anal*
293   *Bioanal Chem* **395**(2), 323-335 (2009).

294   11. J. R. Castro-Suarez et al., "FT-IR Standoff Detection of Thermally Excited Emissions of
295   Trinitrotoluene (TNT) Deposited on Aluminum Substrates," *Appl Spectrosc* **67**(2), 181-186
296   (2013).

297   12. A. Mukherjee, S. Von der Porten, and C. K. N. Patel, "Standoff detection of explosive
298   substances at distances of up to 150 m," *Appl. Opt* **49**(11), 2072-2078 (2010).

299   13. J. C. Carter et al., "Standoff Detection of High Explosive Materials at 50 Meters in Ambient
300   Light Conditions Using a Small Raman Instrument," *Appl. Spectrosc.* **59**(6), 769-775 (2005).

301   14. J. L. Gottfried et al., "Standoff Detection of Chemical and Biological Threats Using Laser-
302   Induced Breakdown Spectroscopy," *Appl. Spectrosc.* **62**(4), 353-363 (2008).

303   15. A. K. Misra et al., "Single-Pulse Standoff Raman Detection of Chemicals from 120 m
304   Distance During Daytime," *Appl. Spectrosc.* **66**(11), 1279-1285 (2012).

305   16. J. E. Parmeter, "The challenge of standoff explosives detection," *Security Technology, 2004.*
306   *38th Annual 2004 International Carnahan Conference on* 355-358 (2004).

307   17. B. E. Bernacki, and M. C. Phillips, "Standoff hyperspectral imaging of explosives residues
308   using broadly tunable external cavity quantum cascade laser illumination," *Proc. SPIE*
309   **7665**(76650I-76650I-76610 (2010).

310   18. W. Ortiz-Rivera et al., "Vibrational spectroscopy standoff detection of threat chemicals,"

311   *Proc. SPIE* **8031**(803129-803129-803110 (2011).

312   19. A. Pettersson et al., "Explosives standoff detection using Raman spectroscopy: from bulk

313   towards trace detection," *Proc. SPIE* **7664**(76641K-76641K-76612 (2010).

314   20. A. Pettersson et al., "Near Real-Time Standoff Detection of Explosives in a Realistic

315   Outdoor Environment at 55 m Distance," *Propellants Explos. Pyrotech* **34**(4), 297-306

316   (2009).

317   21. R. D. W. Alan R. Ford, Darius M. Vunck, Jeremy B. Rose, Thomas B. Blank, Ken R. Pohl,

318   Edwin L. Dottery, Troy A. McVay, Mikella E. Hankus, Ellen L. Holthoff, Paul M.

319   Pellegrino, Steve D. Christesen, Augustus W. Fountain III "Explosives Sensing Using

320   Multiple Optical Techniques in a Standoff Regime with a Common Platform,"

321   *Spectroscopyonline* 6-11 (April 2011).

322   22. N. J. Galán-Freyle et al., "Artificial Intelligence Assisted Mid-Infrared Laser Spectroscopy In

323   Situ Detection of Petroleum in Soils," *Applied Sciences* **10**(4), 1319 (2020).

324   23. G. L. McEneff et al., "Sorbent Film-Coated Passive Samplers for Explosives Vapour

325   Detection Part B: Deployment in Semi-Operational Environments and Alternative

326   Applications," *Scientific Reports* **8**(1), 5816 (2018).

327   24. W. Zhang et al., "Recent Developments in Spectroscopic Techniques for the Detection of

328   Explosives," *Materials* **11**(8), 1364 (2018).

329   25. F. Jin et al., *Chemical and explosive detection with long-wave infrared laser induced*

330   *breakdown spectroscopy*, SPIE (2016).

331   26. R. J. Pell et al., "Quantitative infrared emission spectroscopy using multivariate calibration,"

332   *Anal. Chem* **60**(24), 2824-2827 (1988).

333 27. M. Friedrich, and D. R. T. Zahn, "Emission Spectroscopy: An Excellent Tool for the Infrared

334 Characterization of Textile Fibers," *Appl. Spectrosc.* **52**(12), 1530-1535 (1998).

335 28. M. J. Zuerlein et al., "Modeling thermal emission in dental enamel induced by 9–11 μm laser

336 light," *Appl. Surf. Sci* **127–129**(0), 863-868 (1998).

337 29. R. W. Jones et al., "Chemical Analysis of Wood Chips in Motion Using Thermal-Emission

338 Mid-Infrared Spectroscopy with Projection to Latent Structures Regression," *Anal. Chem*

339 **74**(2), 453-457 (2001).

340 30. T. M. Niemczyk, S. Zhang, and D. M. Haaland, "Monitoring Dielectric Thin-Film

341 Production on Product Wafers Using Infrared Emission Spectroscopy," *Appl. Spectrosc.*

342 **55**(8), 1053-1059 (2001).

343 31. R. Furstenberg et al., "Stand-off detection of trace explosives via resonant infrared

344 photothermal imaging," *Appl. Phys. Lett* **93**(22), - (2008).

345 32. N. Y. Galán-Freyle et al., "Standoff laser-induced thermal emission of explosives," *Proc.*

346 *SPIE* **8705**(870508-870508-870510 (2013).

347 33. A. Figueroa-Navedo et al., "Improved detection of highly energetic materials traces on

348 surfaces by standoff laser-induced thermal emission incorporating neural networks," *Proc*

349 *SPIE* **8705**(87050D-87050D-87011 (2013).

350 34. A. M. Figueroa-Navedo et al., "Chemometrics-enhanced laser-induced thermal emission

351 detection of PETN and other explosives on various substrates," *Journal of Chemometrics*

352 **29**(6), 329-337 (2015).

353 35. F. B. Gonzaga, and C. Pasquini, "Near-Infrared Emission Spectrometry Based on an

354 Acousto-Optical Tunable Filter," *Anal. Chem* **77**(4), 1046-1054 (2005).

355   36. A. Tsuge, Y. Uwamino, and T. Ishizuka, "Applications of Laser-Induced Thermal Emission

356   Spectroscopy to Various Samples," *Appl. Spectrosc.* **43**(7), 1145-1149 (1989).

357   37. O. Primera-Pedrozo et al., "High Explosives Mixtures Detection Using Fiber Optics

358   Coupled: Grazing Angle Probe/Fourier Transform Reflection Absorption Infrared

359   Spectroscopy," *Sens Imaging* **9**(3-4), 27-40 (2008).

360   38. M. Wrable-Rose et al., "Preparation of TNT, RDX and Ammonium Nitrate Standards on

361   Gold-on-Silicon Surfaces by Thermal Inkjet Technology," *Sens Imaging* **11**(4), 147-169

362   (2010).

363   39. R. Infante-Castillo, L. C. Pacheco-Londoño, and S. P. Hernández-Rivera, "Monitoring the

364   α→β solid-solid phase transition of RDX with Raman spectroscopy: A theoretical and

365   experimental study," *J. Mol. Struct* **970**(1–3), 51-58 (2010).

366   40. R. Infante-Castillo, L. Pacheco-Londoño, and S. P. Hernández-Rivera, "Vibrational spectra

367   and structure of RDX and its 13C- and 15N-labeled derivatives: A theoretical and

368   experimental study," *Spectrochim. Acta, Part A: Molecular and Biomolecular Spectroscopy*

369   **76**(2), 137-141 (2010).

370
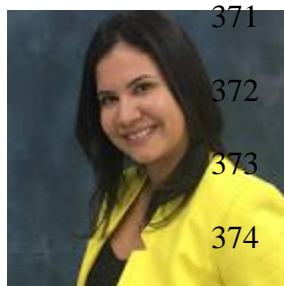
371   **Nataly J. Galán-Freyle** received a BS in chemistry from the University

372   of Cartagena (Colombia), and she received her MS and Ph.D. in Applied

373   Chemistry from the University of Puerto Rico-Mayaguez in 2014 and

374   2016, respectively. Her current research interests include chemical

375   sensors, materials science, nanotechnology, chemometrics and applied spectroscopy.

376
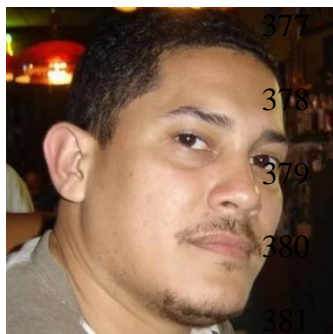
Leonardo C. Pacheco-Londoño received a BS from the University of Cartagena, Cartagena, Colombia, and his MS and Ph.D. in Applied Chemistry from the University of Puerto Rico-Mayagüez, Mayagüez (UPRM). His current research interests include materials science, nanotechnology, chemical sensors, biosensors, chemometrics, artificial intelligence and applied spectroscopy. Currently, he works on the Genetics Department on Biosensors and Macondo Lab Business Entrepreneurship Center on Knowledge Transfer at the Universidad Simon Bolivar, Colombia. He also conducts research on chemical sensors based on quantum cascade lasers, impedance and fluorescence together with the Center for Chemical Sensors (CCD), the Chemical Imaging and Surface Analysis Center (CISAC), and the DHS ALERT-II Center of Excellence for Explosives Research.

Amanda M. Figueroa-Navedo received a BS and MS degree from University of Puerto Rico-Mayagüez. She is currently a Ph.D. candidate at Northeastern University. Her current research interests include data analysis, data science and data visualization for proteomics.

William Ortiz Rivera received a MS and Ph.D. in Applied Chemistry from the University of Puerto Rico-Mayaguez Campus. His current research interests are focused in improvement of analytical methods by employing vibrational techniques for Defense and Security, Pharmaceutical Industries, and agriculture applications.

400

401

John R. Castro-Suarez Research chemist with an MS and a Ph.D. in Applied Chemistry with emphasis on synthesis, characterization and detection of hazardous materials. Experience in the use of Chemometrics software (Multivariate Analysis) such as PLS Toolbox™ for Matlab and Pirouette platform, in the elaboration of multivariate models such as PCA, PLS, DA-PLS, etc. Particularly interested in infrared and Raman spectroscopic data, that allow the design of sensors for the early, rapid, and accurate detection of hazardous substances. Applications to industrial and academic problems in all media such as soils, air and, complex surfaces with little or no sample pre-treatment.

411

412

Samuel P. Hernández-Rivera is a professor of physical chemistry at the University of Puerto Rico-Mayagüez and the UPRM Principal Investigator of the R3-C research, development, education, and training component of the DHS-ALERT Center of Excellence for Explosives Research. He also directs the Center for Chemical Sensors and the Chemical Imaging and Surface Analysis Center. He obtained his BS from UPRM and his Ph.D. from the Johns Hopkins University. His research interests include the use of Raman, FTIR, and MIR laser spectroscopies in fundamental and applied studies, including remote detection of explosives, chemical and biological agents, toxic industrial compounds, and drugs. Other research interests of applied spectroscopy include SERS, SEIRA,

423   TERS, and multivariate analysis and chemometric enhancement of spectroscopic data. Dr.

424   Hernandez is the faculty mentor in charge of the UPRM Student Chapter of the Society for

425   Applied Spectroscopy (SAS).

426

427

428

429

FIGURE CAPTIONS

431 **Fig. 1** Experimental setup of the standoff laser-induced thermal detection (LITE) of HEMs. (a)

432 Optical chopper wheel (OCW) system; (b) Schematic representation of experiment timing for the

433 acquisition time and LITE.

434

435 **Fig. 2** (a) Thermal emission for 500 μg/cm^2 at 4 m of RDX with f_w = 0.1 Hz, d = 4 m, and t_i = 2

436 s; (b) e_A spectra for 18 cycles at 1 Hz and 4 m.

437

438 **Fig. 3** Signal monitoring at 1234 cm^{-1} for (a) f_w = 0.1 Hz, t_i = 2.0 s, and d = 4 m; (b) for f_w = 0.2

439 Hz, t_i = 2 s, and d = 4 m; (c) for f_w = 0.4 Hz, t_i = 2.0 s, and d = 4 m; (d) for f_w = 2.0 Hz, t_i = 2.0 s,

440 and d = 4 m.

441

442 **Fig. 4** (a) e_A spectra for various f_w values for t_i = 2.0 s and d = 4 m; (b) average e_A spectra for

443 various t_i for a total acquisition time of 120 s, f_w = 1.0 Hz and d = 4 m. The min and max spectra

444 of the experiment are shown.

445

446 **Fig. 5** (a) Dependence of the LS diameter for various source-target distances, induced with and

447 without the telescope. Insets: dependence of the temperature increase (ΔT) for various source-

448 target distances (left); reciprocal of LS diameter (right); (b) e_A spectra for various source-target

449 distances for 500 μg/cm^2. Inset: dependence of S/N ratio divided by the nominal surface

450 concentration (C_s) for various source-target distances.

451

(a)

CO₂ Laser

Gold coated mirror

Thermocouple

laser pointer

MCT detector

Interferometer

FT-IR Spectrometer

Sample

Spectrometer window

6.4 cm

1.3 cm

5.1 cm

Counterweight

153.5°

horizon

R = 15.2 cm

10.8 cm

laser spot (LS)

(a)

(b)

t/t₀

0   0.2   0.4   0.6   0.8   1

ON / Off

Acquisition of Emission

LITE

0   60   120   180   240   300   360

Degree (°)

(a)

(b)